

Calcium Sensitivity of Neurotransmitter Release Differs at Phasic and Tonic Synapses

Andrew G. Millar,¹ Robert S. Zucker,² Graham C. R. Ellis-Davies,³ Milton P. Charlton,¹ and Harold L. Atwood¹

¹Department of Physiology, Faculty of Medicine, University of Toronto, Toronto, Ontario, Canada M5S 1A8, ²Department of Molecular and Cell Biology, University of California, Berkeley, California 94720, and ³Department of Pharmacology and Physiology, College of Medicine, Drexel University, Philadelphia, Pennsylvania 19102

The efficacy of synaptic transmission varies greatly among synaptic contacts. We have explored the origins of differences between phasic and tonic crustacean neuromuscular junctions. Synaptic boutons of a phasic motor neuron release three orders of magnitude more quanta to a single action potential and show strong depression to a train, whereas tonic synapses are nearly unresponsive to single action potentials and display an immense facilitation. Phasic and tonic synapses display a similar nonlinear dependence on extracellular $[Ca^{2+}]_o$. We imposed similar spatially uniform intracellular $[Ca^{2+}]_i$ ($[Ca^{2+}]_i$) steps in phasic and tonic synapses by photolysis of presynaptic caged calcium. $[Ca^{2+}]_i$ was measured fluorometrically while transmitter release was monitored electrophysiologically from single boutons in which the $[Ca^{2+}]_i$ was elevated. Phasic synapses released the readily releasable pool (RRP) of vesicles at a much higher rate and with a shorter delay than did tonic synapses. Comparison of several kinetic models of molecular events showed that a difference in Ca^{2+} -sensitive priming of vesicles in the RRP combined with a revision of the kinetic Ca^{2+} -binding sequence to the secretory trigger produced the best fit to the markedly different responses to Ca^{2+} steps and action potentials and of the characteristic features of synaptic plasticity in phasic and tonic synapses. The results reveal processes underlying one aspect of synaptic diversity that may also regulate changes in synaptic strength during development and learning and memory formation.

Key words: synapse; synaptic strength; crayfish; neuromuscular junction; Ca^{2+} sensitivity; priming

Introduction

Transmitter release evoked by a nerve impulse (“synaptic strength”) differs enormously among synaptic connections (Atwood and Karunanithi, 2002). Likewise, short-term plasticity is very diverse, ranging from severe depression to dramatic facilitation. This diversity is linked to functional requirements of the neural circuits in which the connections occur. Many variables contribute to differences in presynaptic performance: ion channel number, properties, and location; synaptic vesicle availability; properties of presynaptic proteins regulating Ca^{2+} dynamics and vesicle exocytosis; and synaptic morphology. For any specific connection, all of these factors must be considered in searching for an explanation of release properties.

Crustacean phasic and tonic glutamatergic motor neurons provide one of the best available examples of synaptic specialization (Kennedy and Takeda, 1965a,b). At synapses of the paired phasic and tonic motor neurons of limb muscles, quantal release from a phasic synapse in response to a single action potential is

typically 100- to 1000-fold greater than for a tonic synapse sharing the same postsynaptic muscle cell (Msghina et al., 1998). Moreover, phasic synapses depress rapidly to repeated activation, whereas tonic synapses display facilitation as great as 100,000% to a 100 Hz train.

Ultrastructural comparisons of individual synaptic boutons revealed that bouton size, synaptic contact area of individual synapses, and number of synapses per bouton are greater for tonic nerve terminals, contrary to the expectation that these features might be positively correlated with initial release probability (King et al., 1996; Msghina et al., 1998). Estimated Ca^{2+} entry per synapse is similar for both types of nerve terminals, and no other differences were found that could account for a 1000-fold difference in probability of quantal release (Msghina et al., 1999) and dramatically different forms of plasticity.

In mammalian cultured neurons, the initial probability of transmitter release is proportional to the size of the readily releasable pool (RRP) (Dobrunz and Stevens, 1997; Schikorski and Stevens, 1997). At crayfish terminals, however, the size of the RRP for tonic synaptic boutons is larger than at phasic synapses, whereas the fractional release per impulse of the RRP is 1500-fold smaller (Millar et al., 2002). One mechanism that might explain the differences between tonic and phasic synapses is the Ca^{2+} dependence of the release process. In this study, we compared release rates during changes in presynaptic intracellular $[Ca^{2+}]_i$ ($[Ca^{2+}]_i$) produced by flash photolysis of caged Ca^{2+} , which elevates $[Ca^{2+}]_i$ rapidly and uniformly throughout terminal

Received Nov. 18, 2004; revised Jan. 27, 2005; accepted Jan. 28, 2005.

This work was supported by grants from the Canadian Institutes of Health Research (CIHR) (H.L.A., M.P.C.), a CIHR graduate scholarship (A.G.M.), grants from the National Institutes of Health (NIH) and National Science Foundation (R.S.Z.), and a grant from the NIH for development of DMNPE-4 (G.C.R.E.-D.). We thank E. Neher for comments on this manuscript and a gift of brilliant sulfaflavine dye, R. Schneggenburger for valuable advice on transmitter release modeling, and M. Hegström-Wojtowicz and R. English for technical assistance.

Correspondence should be addressed to Robert S. Zucker, Department of Molecular and Cell Biology, University of California, Berkeley, CA 94720. E-mail: zucker@berkeley.edu.

DOI:10.1523/JNEUROSCI.4717-04.2005

Copyright © 2005 Society for Neuroscience 0270-6474/05/253113-13\$15.00/0

boutons. For a given $[Ca^{2+}]_i$, release rates at phasic synapses were at least one order of magnitude higher than for tonic synapses. Among several models explored, one in which the secretory trigger binds three Ca^{2+} ions at one site and two Ca^{2+} ions at another site, with explicit priming of vesicles in the RRP, was best able to account for characteristics of responses to $[Ca^{2+}]_i$ steps, single action potentials, and a train of spikes. In this model, tonic and phasic synapses have identical Ca^{2+} sensitivities of the secretory trigger but have very different states of Ca^{2+} -dependent priming.

Materials and Methods

Animals and preparation. Freshwater crayfish (*Procambarus clarkii*; 2–5 cm body length) were obtained from Atchafalaya Biological Supply (Raceland, LA) and maintained under standard laboratory conditions as outlined by Bradacs et al. (1997). We used the carpopodite extensor muscle preparation, which is innervated by two excitatory motor axons: one tonic and one phasic. This preparation has been described in detail previously (Bradacs et al., 1997; Msghina et al., 1998).

Solutions. The preparation was dissected and bathed in a modified Van Harreveld's crayfish solution containing the following (in mM): 205.3 NaCl, 5.3 KCl, 13.5 $CaCl_2$, 2.5 $MgCl_2$, and 10 HEPES buffer, pH 7.4. In some experiments, we further modified the crayfish solution to contain differing concentrations of Ca^{2+} . Solutions contained the following (percentage of normal Ca^{2+} , $[CaCl_2]$, in mM): 0%, 0; 10%, 1.35; 25%, 3.38; 50%, 6.75; 75%, 10.13; 100%, 13.5; 200%, 27; and 800%, 108. Experiments were performed at room temperature ($20 \pm 1^\circ C$).

For "caged calcium" experiments, nerve terminal axons were pressure-injected with a solution containing the following (in mM): 50 dimethoxynitrophenyl-EGTA-4 (DMNPE-4), 37.5 $CaCl_2$, 50 K-HEPES, 13.2 or 6.6 brilliant sulflavine (BS), 1.32 or 0.66 Oregon green 488 BAPTA 6F (OG), and 55 KCl (551–567 mOsm).

UV photolysis. $[Ca^{2+}]_i$ was controlled using the recently developed caged Ca^{2+} chelator DMNPE-4 (Ellis-Davies, 2003). Caged Ca^{2+} was photolyzed with a flash lamp (T.I.L.L. Photonics, Grafelfing, Germany) or a xenon arc lamp (Optikon, Guelph, Ontario, Canada) controlled with a Uniblitz electronic shutter (Vincent Associates, Rochester, NY). Both devices were coupled to an Optiphot 2 upright microscope (Nikon Canada, Mississauga, Ontario, Canada) via a fused silica light guide and a T.I.L.L. Photonics two-port condenser with 400 nm dichroic and 400 nm short-pass filters. The light from the condenser was passed through the microscope to a $40\times$ UV water-dipping objective (Olympus Optical, Tokyo, Japan). This produced a $20 \times 20 \mu m$ square of light in the focal plane of the objective. The remaining port on the condenser was coupled through another light guide to a T.I.L.L. Photonics Polychrome IV monochromator.

When using the flash lamp, we controlled the light intensity by changing the insertion depth of the light guide in the lamp housing. This altered the amount of light entering the light guide by moving the aperture out of the focal plane of the light beam. Gradations were marked on the light guide adapter corresponding to the intensity of light at the output of the objective, which was measured using a fast photodiode in the focal plane of the objective. To monitor flash duration and intensity during experiments, we placed a photodiode at a small opening in the two-port condenser; its output was digitized concurrently with imaging and electrophysiological data.

$[Ca^{2+}]_i$ measurement. We estimated $[Ca^{2+}]_i$ in boutons using the two-dye, dual-excitation wavelength technique of Oheim et al. (1998). This technique measures the ratio of the fluorescence of a single-wavelength, Ca^{2+} -sensitive dye to that of a Ca^{2+} -insensitive dye to correct for dye concentrations and path length. We used OG as the Ca^{2+} -sensitive dye and BS as the Ca^{2+} -insensitive dye. Both dyes were pressure-injected into presynaptic terminals along with caged Ca^{2+} . Injected materials were allowed to diffuse to terminal boutons for 30 min. Fluorescence was measured by alternately exciting OG and BS at wavelengths of 480 and 420 nm, respectively, using the T.I.L.L. Photonics monochromator. Fluorescence emission (535 ± 20 nm) was measured by the T.I.L.L. Photonics photodiode system, and the output was digitized at

10 kHz using a PowerLab data acquisition system (AD Instruments, Colorado Springs, CO). Fluorescence intensities were corrected for tissue fluorescence by subtracting backgrounds measured from a muscle region adjacent to the filled nerve.

$[Ca^{2+}]_i$ calibrations. Fluorescence measurements were converted to $[Ca^{2+}]_i$ by standard methods (Grynkiewicz et al., 1985) using the ratio of OG fluorescence intensity to excitation at 480 nm divided by BS fluorescence intensity to excitation at 420 nm for three calibration solutions containing no Ca^{2+} (R_{min}), 5 mM Ca^{2+} (R_{max}), and 4.5 μM Ca^{2+} (R_{mid}). Solution fluorescence was measured from a microcuvette chamber (20 μm path length; VitroCom, Mountain Lakes, NJ) placed in the focal plane of the microscope objective, with background subtraction of the cuvette fluorescence filled with water.

R_{min} was measured for a solution containing the following (in mM): 10 K_2H_2 -DMNPE-4, 1.32 BS, 0.132 OG, 15 HCl, 50 K-HEPES, 10 K_2 -EGTA, and 175 KCl, pH 7.4. The HCl was added to neutralize the DMNPE-4, which was provided in highly basic tetrapotassium form; this produced 15 mM KCl, and the K_4 -DMNPE-4 stock solution contained another 5 mM KCl (calculated from its degree of protonation estimated from the pH of a diluted solution). R_{max} was measured in a solution of (in mM): 10 CaK_2 -DMNPE-4, 1.32 BS, 0.132 OG, 50 K-HEPES, 5 $CaCl_2$, and 185 KCl plus 20 mM KCl from the K_4 -DMNPE-4, pH 7.4. The ionic strength of these solutions was 280 mM, the same as for crayfish Ringer's solution. R_{mid} was measured in a solution containing the Ca^{2+} buffer 1,3-diaminopropane-2-ol- N,N' -tetraacetic acid (DTPA; Sigma, St. Louis, MO) to control the $[Ca^{2+}]_i$ at an intermediate concentration near the K_D of OG. The solution contained the following (in mM): 10 CaK_2 -DMNPE-4, 1.32 BS, 0.132 OG, 20 CaK_2 -DTPA, 30 K_3 H-DTPA, 50 K-Trizma, pH 8.0, and 20 KCl produced by neutralization, with a slightly hypertonic ionic strength of 316 mM. At this pH and ionic strength, DTPA has an effective K_D for Ca^{2+} of 6.9 μM (interpolated from Grimes et al., 1963; Neher and Zucker, 1993; Ohnuma et al., 2001), and the free $[Ca^{2+}]_i$ of the solution should be 4.5 μM (confirmed by measurement with Ca^{2+} ion-selective electrodes; Microelectrodes, Londonderry, NH). If CaK_2 -DMNPE-4 is made stoichiometrically, it will affect neither pH nor the free $[Ca^{2+}]_i$; therefore, it was produced by titrating DMNPE-4 with Ca^{2+} using Ca^{2+} -sensitive electrodes. The pCa of a stock solution containing everything except the DMNPE-4 and the dyes was also checked and confirmed with ion-sensitive electrodes.

Averaging several calibrations, R_{max}/R_{min} was 5.32, whereas without DMNPE-4, R_{max}/R_{min} was ~ 10 , so DMNPE-4 appears to partially quench OG fluorescence, particularly when bound to Ca^{2+} (cf. Zucker, 1992), and to reduce its sensitivity to Ca^{2+} . Typical parameter values of R_{max} , R_{min} , and R_{mid} were 4.84, 0.91, and 2.9, respectively, corresponding to a K_D of 4.4 μM . This is substantially higher than the nominal OG K_D of 3 μM . From the effect of ionic strength on similar indicators (cf. Grynkiewicz et al., 1985; Zhong et al., 2001), a K_D of 4.5 μM would be expected, and we used this value for converting fluorescence ratios to $[Ca^{2+}]_i$.

The calibration solutions contained DMNPE-4, OG, and BS in the same ratios (but one-tenth of the concentrations) as the solutions in injection pipettes. Two-dye $[Ca^{2+}]_i$ measurements require that the concentration ratio of the dyes remain constant and equal to that used for calibrations. However, OG and BS diffuse at different rates (Oheim et al., 1998); therefore, their ratio is likely to be variable in different boutons and at different times and not equal to that of calibration solutions. This problem, along with variations in the light source spectrum, results in different values of R_{min} in each experiment. However, R_{max}/R_{min} is unaffected by the concentration ratio. The free $[Ca^{2+}]_i$ in our injection solution equals the resting $[Ca^{2+}]_i$ in axons (100 nM), which is 2% of the K_D of OG, so the initial fluorescence ratio should be within 2% of the range from R_{min} to R_{max} . We thus used the initial resting fluorescence ratio as R_{min} for converting R to $[Ca^{2+}]_i$ in each experiment.

We tested for effects of bleaching by photolysis flashes using the Ca-free or Ca-loaded solutions for determining R_{min} and R_{max} . A full-intensity flash caused a little less than 5% bleaching, which would not introduce much error into estimates of $[Ca^{2+}]_i$, because this flash brought $[Ca^{2+}]_i$ into the middle of the Ca sensitivity range of OG in which bleaching effects are least consequential.

Predicting Ca(t) during the flash artifact and the effect of our flashes. To analyze how putative reaction schemes for transmitter release would respond to the time course of $[Ca^{2+}]_i$, $Ca(t)$, we had to replace the artifact in the $Ca(t)$ recording with an estimated time course of $Ca(t)$. This was especially important because, for large $[Ca^{2+}]_i$ increases, most transmitter release occurred during the first 50 ms after the flash, when the artifact obscured the $Ca(t)$ measurement. The $Ca(t)$ measurement missed the expected “spike” in $Ca(t)$ that occurs during the flash (Zucker, 1994; Ellis-Davies, 2003) because of saturation of the detector during the flash. The time course of the saturation artifact over the 50 ms after the beginning of the flash was similar in boutons that contained just the indicators (data not shown) and in boutons that contained indicators and DMNPE-4 except for the elevated baseline after the flash in DMNPE-4-containing boutons.

To calculate the temporal profile of $Ca(t)$ during and immediately after the flash, we used a simplified reaction scheme for DMNPE-4 similar to that outlined by Ellis-Davies et al. (1996). It included a one-step photolysis process and no Mg^{2+} binding (which is negligible for DMNPE-4) or binding of Ca^{2+} to photoproducts (which has negligible effects in the presence of endogenous Ca^{2+} buffers). The evolution of photolysis of DMNPE-4 was estimated by convolution of the measured time course of the photolysis flash (recorded from reflected light with a photodiode) with the photolysis rate of DMNPE-4. The photolysis efficiency of the flash for DM-nitrophen was estimated using small droplets under oil of a mixture of DM-nitrophen and fluo-3, as described by Zucker (1994), and converted to an efficiency for DMNPE-4 by accounting for the relative UV absorbances and quantum efficiencies of the two caging compounds.

This temporal reduction in [DMNPE-4] was used to drive a series of differential equations representing the binding of DMNPE-4 to Ca^{2+} and an endogenous cytoplasmic Ca^{2+} buffer and removal of free Ca^{2+} by a first-order pump. The equations were solved using a BASIC program and first-order Euler methods. The affinity of DMNPE-4 for Ca^{2+} depends on pH and ionic strength; we used a value of 48 nM, the affinity at pH 7.2 in mammalian ionic strength and approximately appropriate for the higher ionic strength (~ 280 mM) of crayfish cytoplasm, and a pH of ~ 7.3 (Ellis-Davies et al., 1996), which have opposite effects on affinity. We assumed an on rate of 1.7×10^7 M/s, the value for the chemically similar compound nitrophenyl-EGTA (Ellis-Davies et al., 1996). Measurement of the fluorescence intensity of indicators coinjected with the DMNPE-4 in boutons set the initial unphotolyzed DMNPE-4 concentration at 2–4 mM. Ca loading of the injection solution was 75%, resulting in a free $[Ca^{2+}]_i$ of 106 nM. This is close to the resting $[Ca^{2+}]_i$ in motor nerve terminals (Delaney et al., 1991), so it was assumed that pumping did not alter the DMNPE-4 Ca^{2+} loading before photolysis.

Endogenous Ca^{2+} buffering has a buffer ratio of 600 in crayfish opener motor neuron terminals (Tank et al., 1995). Because the endogenous buffer is not saturated by several micromolar $[Ca^{2+}]_i$, implying a high capacity, we represented it as 10 mM Ca^{2+} -binding buffer sites with 16 μ M Ca^{2+} affinity, although less buffer of higher affinity remains possible. We assumed an on rate of 5×10^7 M/s, one-half that of the endogenous Ca^{2+} buffer in mammalian chromaffin cells (Xu et al., 1997), to account for higher crayfish ionic strength. Simulations included the effects of Ca^{2+} binding to OG, with affinity of 4.5 μ M and on rate of 1×10^8 M/s (typical for BAPTA derivatives, but reduced for crayfish) (Kao and Tsien, 1988; Ellis-Davies et al., 1996). Its concentration was set to 2.6% that of DMNPE-4, as in the injection mixture, or 52–104 μ M, as determined by the range of fluorescence intensities of filled boutons compared with the fluorescence of a known concentration in microcuvettes containing cytoplasm-like fluid and correcting for the relative thickness of the cuvettes and boutons.

Ca^{2+} was removed to a steady-state level of 100 nM by a nonsaturating pump at a rate of 0.12/ms, which pumps Ca^{2+} off the native buffer with a time constant of 5 s, as observed experimentally (Tank et al., 1995).

Simulations of the effects of a bright flash on $Ca(t)$ were compared with $Ca(t)$ measurements to a full flash in a typical experiment (see Fig. 5A) and found to match closely for an assumed bouton DMNPE-4 concentration of 2.75 mM and Ca indicator concentration of 72 μ M, after subsidence of the flash artifact. This is 5% of the concentration of mate-

rial in the injection pipette, which is typical of the level of filling achievable in boutons within a few hundred micrometers of the injection site; moreover, the dye concentration needed for simulations to match measurements is right in the middle of our estimate of dye concentration from fluorescence intensity (52–104 μ M). The correspondence between simulations and measurements provides an independent check of our calibration of the Ca^{2+} sensitivity of OG, as well as a check of our estimate of the photolysis efficiency of our flash apparatus. These concentrations of DMNPE-4 and OG were therefore selected for simulations of a series of eight light flashes at between 15 and 100% of the full intensity flash, which covered the full range of $Ca(t)$ measurements in our experiments. The $Ca(t)$ waveforms generated by these simulations (see Fig. 5A) were used to predict the responses of reaction schemes used to represent various molecular schemes for transmission at phasic and tonic synapses.

The highest $[Ca^{2+}]_i$ level achieved by photolysis in our experiments was ~ 3.2 μ M. This value seems low but actually matches our predictions, as outlined below. A 3 mM concentration is far less than the levels exceeding 100 μ M typically achieved in cells perfused with DM-nitrophen. For example, when mammalian cells are perfused with an Mg^{2+} -free solution, the effective Ca^{2+} affinity for DM-nitrophen remains at 5 nM, and the DM-nitrophen can be almost fully loaded with Ca^{2+} and still leave $[Ca^{2+}]_i$ at 100 nM. Then whatever amount of DM-nitrophen is photolyzed (e.g., 80% of 10 mM = 8 mM), the same amount of free $[Ca^{2+}]_i$ is released onto a native buffer with a typical buffer ratio of 50 (for most cells), resulting in a $[Ca^{2+}]_i$ increase to 160 μ M (Neher and Zucker, 1993). When injecting nerve terminals, the Mg^{2+} cannot easily be removed from boutons 100–300 nm away, and this Mg^{2+} would displace Ca^{2+} from DM-nitrophen, leading to a “loading transient” that itself would activate secretion and might exhaust the RRP before flash experiments begin (Neher and Zucker, 1993). Therefore, we used Mg^{2+} -tolerant DMNPE-4, but its affinity for Ca^{2+} is one-tenth that of DM-nitrophen, and it can only be 75% loaded with Ca^{2+} ; otherwise, resting $[Ca^{2+}]_i$ is increased too much. The quantum efficiency and absorbance of DMNPE-4 are similar to those of DM-nitrophen, so a flash would photolyze a similar fraction of DMNPE-4 to release approximately three-fourths as much Ca^{2+} . However, we can only fill boutons by injection with one-fourth the chelator concentration often used when perfusing whole cells. Moreover, crayfish cytoplasm has 12 times the buffer capacity of typical mammalian cells. These considerations lead to the expectation that we should be able to elevate $[Ca^{2+}]_i$ to ~ 2.5 μ M.

Predicting Ca(t) during an action potential. Vesicle release is triggered by the local increase in $[Ca^{2+}]_i$ in “microdomains” because of the entry of Ca^{2+} ions through clusters of Ca^{2+} channels with individual “nanodomains” that overlap (Zucker et al., 1999; Augustine et al., 2003). In this situation, the local $Ca(t)$ will follow closely the time course of the summed Ca^{2+} fluxes through the individual channels in the cluster, which corresponds to the macroscopic Ca^{2+} current (Roberts, 1994). Transmitter release at crayfish motor nerve terminals is governed by Ca^{2+} entry through P-type Ca^{2+} channels (Araque et al., 1994; Blundon et al., 1995), the kinetics of which closely resemble those that have been studied exhaustively at the squid giant synapses (Wright et al., 1996). We therefore used a kinetic model of the squid presynaptic Ca^{2+} current (Llinás et al., 1981) as modified by Llinás et al. (1982), with the temperature set to 19°C, typical of the present experiments. The kinetic equations were driven with an action potential waveform recorded from motor nerve axons at 19°C. (No difference was observed between phasic and tonic axons.) The resulting $Ca(t)$ was almost exactly described by a Gaussian curve, so a closely fitting Gaussian curve ($\sigma = 250$ μ s) was used to represent $Ca(t)$. The peak $[Ca^{2+}]_i$ amplitude reached during an action potential depends critically on the Ca^{2+} flux per channel, the number of Ca^{2+} channels opening near a docked vesicle, their exact distances from the secretory trigger, and the binding kinetics and mobilities of endogenous buffers (Tang et al., 2000; Matveev et al., 2002, 2004). Because none of these is known with sufficient precision, the peak $[Ca^{2+}]_i$ amplitude produced by an action potential at the secretory trigger remained a free parameter (cf. Bollmann et al., 2000; Schneggenburger and Neher, 2000).

Electrophysiology. Conjointly with measuring $[Ca^{2+}]_i$, neurotransmitter release was assayed by focal extracellular recording at visualized phasic and tonic nerve terminal boutons, using procedures described by

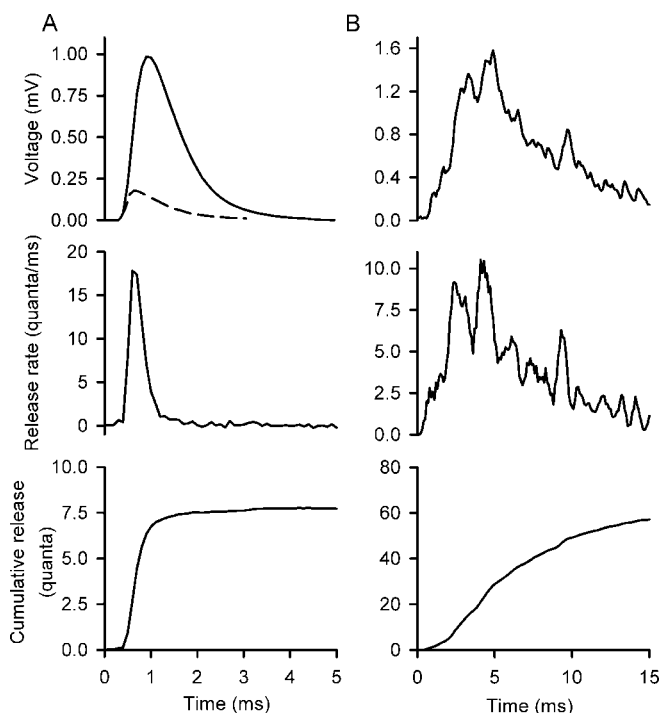


Figure 1. Deconvolution of release rates in a phasic terminal. *A*, An EJC (solid line) evoked by an action potential and an averaged mEJC (dashed line) are shown in the top trace, followed by the calculated release rate of quantal events in the middle trace and cumulative number of quanta in the bottom trace. *B*, The response to a flash is shown in the top trace, the release rate calculated by deconvolution with mEJCs is shown in the middle trace, and cumulative release is shown in the bottom trace, to a step $[Ca^{2+}]_i$ elevation to $3 \mu M$.

Msghina et al. (1998). Loose macropatch recordings (Dudel, 1981; Wojtowicz et al., 1994; Cooper et al., 1995) of the presynaptic nerve terminal action potentials and excitatory junction currents (EJCs) were obtained in current-clamp mode from single visualized tonic and phasic terminal boutons. In this mode, the extracellular voltage provides a measure of local postsynaptic current density. As first demonstrated by Ravin et al. (1997), a crayfish bouton can be effectively illuminated and visualized to measure $[Ca^{2+}]_i$ while a macro-patch electrode is in place to measure transmitter release from the same bouton.

Release rate determination. To estimate rates of neurotransmitter release in phasic and tonic boutons, we applied a procedure based on Fourier transforms of both EJCs and miniature EJCs (mEJCs) recorded from the same bouton (Van der Kloot, 1988). We used the equation $F[n(t)] = F[EJC]/F[mEJC]$, where $F[EJC]$ is the Fourier transform of an evoked response, $F[mEJC]$ is the Fourier transform of the averaged quantal events, and $F[n(t)]$ is the Fourier transform of the quantal release rate at time t . The inverse Fourier transform of $F[n(t)]$ yields $n(t)$. As shown in Figure 1*A*, deconvolution of an EJC with averaged mEJCs produced a maximum release rate of 17.5/ms, and cumulative release of 7.8 quanta was estimated, which compares well with the quantal content of 7.5 obtained by dividing the EJC area by the mEJC area. Deconvolution of responses to a flash was also used to estimate release rate versus time after the flash; an example is shown in Figure 1*B*.

To evaluate our deconvolution algorithm, we used the procedure proposed by Van der Kloot (1988), in which a predicted evoked response is reconstructed from the calculated release rate and compared with the actual response. We used the equation: $F[\text{pred}] = F[mEJC] \times F[n(t)]$, where $F[\text{pred}]$ is the Fourier transform of the predicted evoked event; the inverse Fourier transform of this function did in fact reproduce the actual evoked event. An additional test of the procedure was conducted by constructing an artificial EJP from a series of mEJPs designated as occurring at predetermined times. Deconvolution analysis reproduced the predetermined rate of release and total number of quantal events. Additional tests were conducted on flash-evoked responses in which quanta

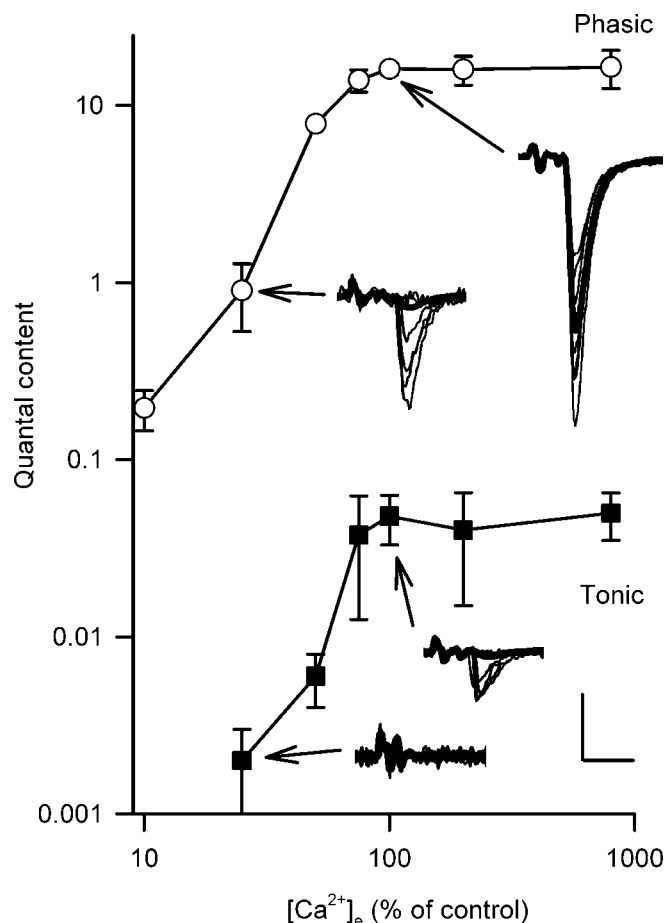


Figure 2. Sensitivity of neurotransmitter release to external Ca^{2+} concentration. Focal recordings of quantal transmitter release were made at individual phasic and tonic boutons with stimulation at 0.2 Hz as $[Ca^{2+}]_e$ was varied from 10 to 800% of control (13.5 mM). Quantal contents are given for various values of $[Ca^{2+}]_e$. Phasic terminals released many more quanta at all values of $[Ca^{2+}]_e$. Sample EJC traces are shown for selected data points. Thick traces indicate the average EJC; thin lines are representative EJCs. Calibration: 0.2 mV, 2 ms. Error bars indicate SEM.

could be detected and counted individually. Our procedure produced release rates and total quantal counts that agreed with estimates derived directly from measuring the time of occurrence of each event. Cumulative quantal contents to an action potential or for a defined period after a flash were estimated by integrating the calculated release rates or by counting quanta in responses where they were individually distinguishable.

Data collection and analysis. Electrophysiological and photometric signals were low-pass-filtered at 5 kHz using a 2004-F Signal Conditioner (Intronix Technologies, Toronto, Ontario, Canada) and subsequently digitized at 10 kHz using a PowerLab/4sp data acquisition system (AD Instruments). Data analysis was performed using Excel (Microsoft, Redmond, WA), Mathematica (Wolfram Research, Champaign, IL) was used for the Fourier analysis.

Modeling molecular reaction schemes. First-order Euler approximations of differential equations were implemented in IgorPro 5.01 (WaveMetrics, Lake Oswego, OR), based on algorithms kindly provided by R. Schneggenburger (Max-Planck Institute for Biophysical Chemistry, Göttingen, Germany). Parameters were varied over a wide range, and we present those giving the best fits of multiple response characteristics to data as determined by eye. Some fits are imperfect; for these, it was found that parameter choices improving fits for one characteristic resulted in worse fits for other characteristics. Thus, an (arbitrary) choice was sometimes made as to which characteristics to fit best.

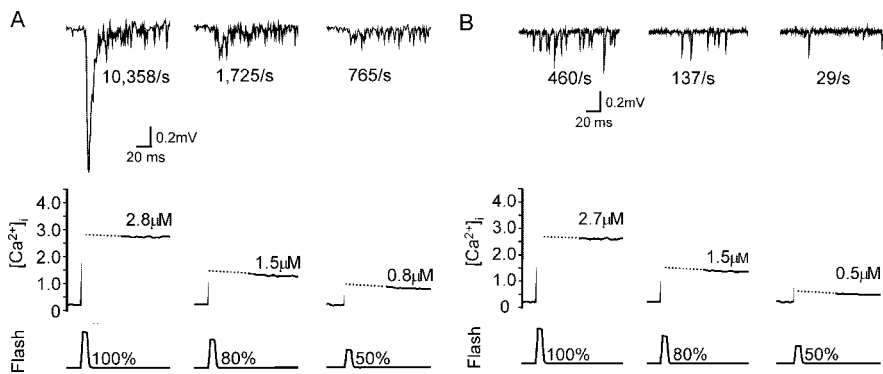


Figure 3. EJCs of phasic and tonic boutons evoked by different $[Ca^{2+}]_i$ steps. **A**, A phasic bouton loaded with DMNPE-4 was exposed to three UV flashes of varying intensity. Postsynaptic responses to flashes are shown in the top trace, $[Ca^{2+}]_i$ responses are shown in the middle trace, and flash intensity is shown in the bottom trace. **B**, Responses to a similar series of flashes in a tonic bouton, showing much less intense release.

Results

Dependence of transmitter release on extracellular $[Ca^{2+}]_e$

A preliminary experiment compared the dependence of evoked transmitter release on extracellular Ca^{2+} concentration ($[Ca^{2+}]_e$). As unbuffered $[Ca^{2+}]_e$ was increased from 0 to 800% of the standard control value (13.5 mM), quantal content increased from close to zero to a maximum value, which was attained at approximately the standard value of $[Ca^{2+}]_e$ (Fig. 2). All recordings contained presynaptic nerve terminal potentials; this indicated that blockage of release was not caused by failure of action potential propagation (Fig. 2, inset). For both phasic and tonic boutons, quantal content (estimated from the ratio of average EJP amplitude to average mEJP amplitude) increased at higher values of $[Ca^{2+}]_e$ with a slope of ~ 3 in a double-logarithmic plot (Fig. 2). At 100% $[Ca^{2+}]_e$, phasic nerve terminal boutons produced multiquantal responses with a quantal content of 16.1 ± 1.2 (mean \pm SE; $n = 6$); responses of tonic boutons had a mean quantal content of 0.05 ± 0.15 ($n = 8$). Increasing $[Ca^{2+}]_e$ beyond 100% resulted in no further increases in quantal content for phasic or tonic terminal boutons, probably reflecting saturation of Ca^{2+} influx through Ca^{2+} channels, a serious limitation of this technique. At lower $[Ca^{2+}]_e$, quantal content from phasic terminal boutons was at least two orders of magnitude higher than for tonic boutons. Because the number of phasic or tonic synapses per micrometer of nerve terminal typically differs by less than a factor of 2 (King et al., 1996), macropatch electrodes recorded from similar numbers of active zones of phasic and tonic motor neurons. The large differences in quantal content of phasic and tonic terminals at all concentrations of external Ca^{2+} may arise from differences in the Ca^{2+} sensitivity of the transmitter release process.

Dependence of transmitter release on intracellular $[Ca^{2+}]_i$

As a more direct measure of the Ca^{2+} sensitivity of the exocytic process, we used photolysis of the caged Ca^{2+} compound DMNPE-4 to control presynaptic $[Ca^{2+}]_i$. UV flashes of varying intensities produced a range of $[Ca^{2+}]_i$ elevations, which were estimated by ratiometric fluorimetry using the indicator dyes OG and BS (Oheim et al., 1998) while quantal release rates were recorded. The latter were estimated by deconvolution of the postsynaptic currents with an averaged mEJC recorded from the same bouton. A typical example from a phasic bouton is shown in Figure 3A. This bouton was exposed to three flashes (separated in time by 5 min) at 100, 80, and 50% strength; $[Ca^{2+}]_i$ was elevated

to 2.8, 1.5, and 0.8 μM , respectively. Before the flashes, the spontaneous transmitter release rate was ~ 2 quanta/min. The elevation to 2.8 μM resulted in a rapidly developing exocytic burst with maximum release rate of 12,000 quanta/s, followed by continued release of individual quanta for several hundred milliseconds. The exocytic burst released ~ 60 quanta, suggesting that the RRP was secreted within 25 ms. For the first 50 ms after the burst, release persisted at 280 quanta/s. We interpret this persistent release as reflecting refilling of the RRP from a reserve pool of vesicles, with release of these vesicles soon after their entrance into the RRP. The elevation of $[Ca^{2+}]_i$ to 1.5 μM resulted in a smaller exocytic burst, with a peak release rate of 1050 quanta/s, followed by continuing release at 250 quanta/s. Elevating $[Ca^{2+}]_i$ to 0.8 μM evoked a small exocytic burst with peak release rate of 320 quanta/s and continuing release at 200/s after the burst.

Results of comparable UV flashes applied to tonic boutons are illustrated in Figure 3B. In this typical tonic bouton, three UV flashes separated by 5 min were applied at strengths of 100, 80, and 50%, elevating $[Ca^{2+}]_i$ to 2.7, 1.6, and 0.5 μM , respectively. At rest, spontaneous transmitter releases were infrequent, approximately one or two per minute. The 2.7 μM $[Ca^{2+}]_i$ step resulted in desynchronized release of quanta for ~ 200 ms, at a maximum rate of 205 quanta/s. The 1.5 μM $[Ca^{2+}]_i$ elevation elicited a shower of quanta at a lower maximum rate of 137 quanta/s continuing for ~ 150 ms. The 0.5 μM $[Ca^{2+}]_i$ step resulted in the release of very few quanta, at a peak rate of 29 quanta/s.

The results of 10 experiments on tonic synapses and 12 on phasic synapses similar to those shown in Figure 3 were compiled to examine the relationship between flash-elevated $[Ca^{2+}]_i$ and transmitter release. Figure 4A shows the relationship between release rate for tonic and phasic boutons and $[Ca^{2+}]_i$ measured immediately after the flash artifact (at 50 ms). At $[Ca^{2+}]_i$ of > 1.5 μM , phasic release rates (open symbols) reached levels as high as 10,000/s. For values of $[Ca^{2+}]_i$ between 0.25 and 1.5 μM , release rates for phasic boutons were an order of magnitude higher than for tonic boutons for a given $[Ca^{2+}]_i$ level. At maximum $[Ca^{2+}]_i$ levels reached in this study (3 μM), release rates at phasic boutons were nearly 100 times higher than at tonic boutons.

RRP sizes were previously estimated for crayfish tonic and phasic boutons (Millar et al., 2002) as 130 ± 23 and 58 ± 5.6 , respectively. In Figure 4B, we divided the total number of quanta released in the first 30 ms by these mean RRP sizes so that the ordinate represents the percentage of the typical RRP released during this period. At all $[Ca^{2+}]_i$ levels of > 2 μM , phasic boutons released most of the RRP within 30 ms. At $[Ca^{2+}]_i$ values between 0 and 1.5 μM , the percentage of RRP released rose rapidly until reaching its maximum. At tonic synapses, responses to $[Ca^{2+}]_i$ steps did not display an early clustering of release characteristic of an exocytic burst. Correspondingly, the percentage of RRP released in the first 30 ms rose gradually with increasing $[Ca^{2+}]_i$, reaching only 6–7% of the mean RRP as $[Ca^{2+}]_i$ approached 3 μM . For a given $[Ca^{2+}]_i$ level, the fraction of the RRP released within 30 ms was ~ 10 times higher for phasic than for tonic boutons.

Transmitter release to $[Ca^{2+}]_i$ steps was also considerably more sluggish at tonic synapses. Figure 4C plots the time from the

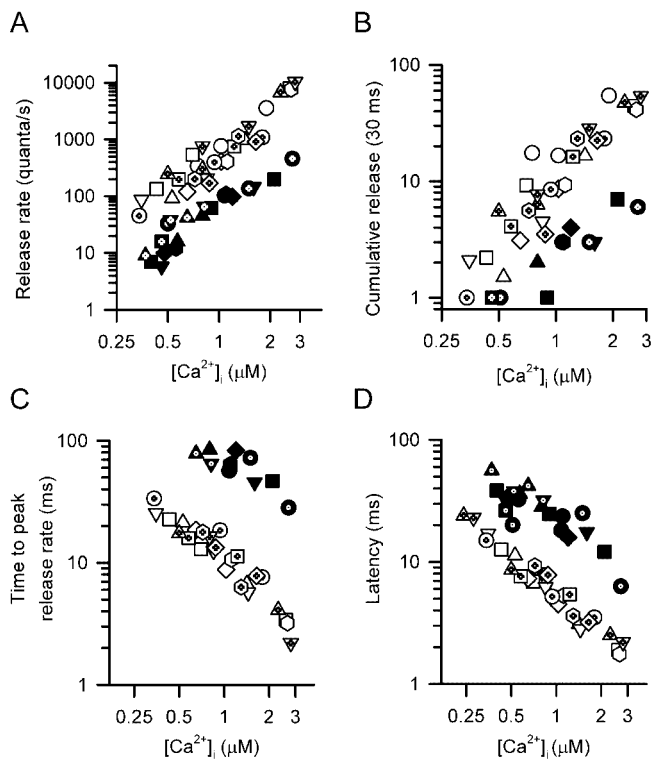


Figure 4. Relationship between $[Ca^{2+}]_i$ and transmitter release at phasic and tonic terminals. Trials from phasic experiments are shown with open symbols ($n = 12$; each symbol represents data from a different preparation), whereas trials from tonic experiments are shown with filled symbols ($n = 10$). **A**, Maximum release rate plotted versus $[Ca^{2+}]_i$, measured at 50 ms. **B**, Percentage of average RRP released by a flash within 30 ms, plotted against $[Ca^{2+}]_i$. **C**, Time to peak rate of release versus amplitude of the $[Ca^{2+}]_i$ step. **D**, Latency from flash to first quantal release versus amplitude of the $[Ca^{2+}]_i$ step.

flash to when the release rate reached its maximum. Phasic synapses released their RRP briskly, with peak release rates occurring at 20 ms for $[Ca^{2+}]_i$ steps to $0.5 \mu M$ to as early as 2 ms after the flash for $[Ca^{2+}]_i$ steps to near $3 \mu M$. At tonic synapses where few quanta were released, the time to peak frequency could be estimated only approximately: it occurred as late as 80 ms after a $[Ca^{2+}]_i$ step to $0.5 \mu M$ and at ~ 30 ms after a step to near $3 \mu M$.

Finally, the minimum synaptic delay, or time to the release of the first quantum, was also much shorter at phasic synapses (Fig. 4D). At both types of synapses, release began sooner for larger $[Ca^{2+}]_i$ steps. Release at phasic synapses started 7–8 ms after a $[Ca^{2+}]_i$ step to $0.5 \mu M$ or < 2 ms after a $3 \mu M$ step. At tonic synapses, release began 30 ms after a step to $0.5 \mu M$ and at least 5 ms after a step to near $3 \mu M$.

We also performed experiments on three pairs of boutons to estimate the “thresholds” of $[Ca^{2+}]_i$ at which quantal release increases above baseline spontaneous levels. Low-intensity pulses of uncaging illumination from a xenon light source were delivered through appropriate neutral density filters and graded to produce several levels of $[Ca^{2+}]_i$ in each selected bouton while simultaneously recording quantal events at the same bouton. The threshold value of $[Ca^{2+}]_i$ at which an increased rate of quantal events could be detected was 0.4 – $0.5 \mu M$ for both synapse types. The threshold value for a given bouton was independent of the rate of rise or final value of $[Ca^{2+}]_i$. The threshold values so estimated are considerably lower than the $[Ca^{2+}]_i$ values esti-

mated for Ca^{2+} “nanodomains” or “microdomains” around opened synaptic Ca^{2+} channels (Neher, 1998). The observation suggests that spontaneous release of vesicles does not increase markedly for values of $[Ca^{2+}]_i$ near the normal resting level, which is thought to be in the range of 100 – 200 nM for these neurons (Msghina et al., 1999).

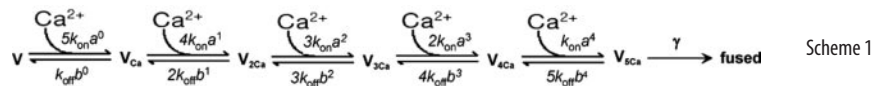
Molecular reaction schemes of the release process

Phasic synapses are much more sensitive to modest $[Ca^{2+}]_i$ elevations than tonic synapses. We wanted to know whether the different responses of phasic and tonic synapses to step rises in $[Ca^{2+}]_i$ could quantitatively explain the large differences in quantal content evoked by action potentials. We also wanted to know what type of molecular reaction scheme might underlie the differences in physiology between phasic and tonic synapses.

These questions are linked because relating our findings to spike-evoked release requires application of a kinetic model of the molecular responses to $[Ca^{2+}]_i$ steps. The question is whether the likely time course and magnitude of $[Ca^{2+}]_i$ changes during an action potential would be expected to evoke quantal contents differing by up to three orders of magnitude when most aspects of the $[Ca^{2+}]_i$ step responses differed by only one order of magnitude at phasic and tonic synapses. Our approach to this problem follows that of others (Bollmann et al., 2000; Schneggenburger and Neher, 2000): to build a molecular model of the secretory response to step $[Ca^{2+}]_i$ rises and to test whether the model can be driven by a reasonable temporal profile of local $[Ca^{2+}]_i$ to release quanta with the time course evoked by an action potential.

Positive cooperativity model, with different secretory triggers

We began with the reaction scheme of Heidelberger et al. (1994), devised to account for transmitter release at retinal bipolar synapses, and later extended (Bollmann et al., 2000; Schneggenburger and Neher, 2000) to describe results at the calyx of Held and hair cells (Beutner et al., 2001). The scheme has up to five Ca^{2+} ions binding sequentially to identical sites on a secretory trigger, with the possibility of positive cooperativity increasing the affinity of successive binding steps, and ending in a Ca^{2+} -independent step representing the kinetics of vesicle fusion:



Here, V refers to vesicles in the RRP, which at rest are unbound by Ca^{2+} ions in state V and are driven by sequentially binding Ca^{2+} ions until all available sites are occupied, whereupon secretion of the activated vesicle occurs within a time determined by γ . Positive cooperativity is expressed either by increasing the successive binding rates by factors of $a > 1$ or decreasing successive dissociation rates by factors of $b < 1$.

The first question was whether Scheme 1 could describe the characteristics of phasic and tonic synapses to step rises in $[Ca^{2+}]_i$. We addressed this question by driving the reactions with a time-dependent $[Ca^{2+}]_i$, $Ca(t)$, calculated for a series of eight flashes that produced $[Ca^{2+}]_i$ changes ranging from those obtained with our dimmest flash to our brightest flash. Because of saturation of the photodiode, which distorted the $Ca(t)$ measurement for up to 50 ms after the flash, we had to calculate the change in $[Ca^{2+}]_i$ for the first 50 ms. Thus, we actually drove the model with a series of $Ca(t)$ profiles (Fig. 5A) that were fitted to $Ca(t)$ measurements after subsidence of the flash artifact and

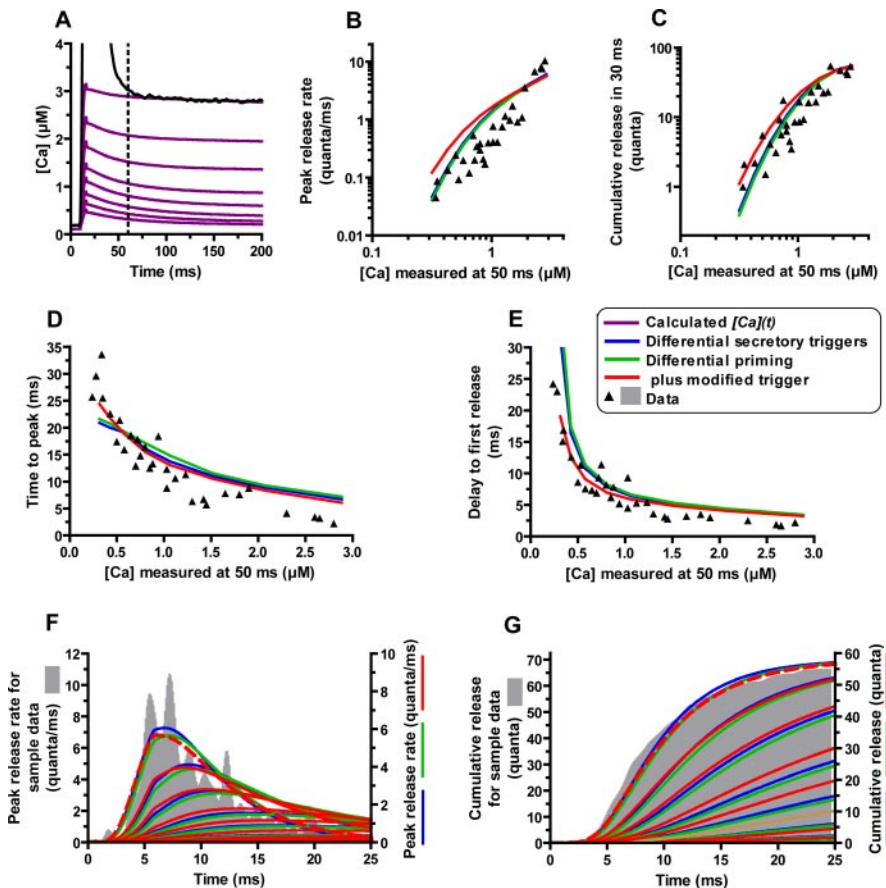


Figure 5. Predicted characteristics of phasic synapse responses to Ca^{2+} steps of three molecular schemes and comparison with experimental data. **A**, Purple lines represent $\text{Ca}(t)$ calculated from simulations of DMNPE-4 photolysis to flashes of varying intensity (100, 80, 65, 50, 40, 30, 22, and 15% of full intensity), reaching levels of 2.9, 2.1, 1.5, 1.1, 0.80, 0.58, 0.43, and 0.31 μM , respectively, at 50 ms after the flash (dotted line). The solid black line is a $\text{Ca}(t)$ measurement to a full-intensity flash from a bouton containing DMNPE-4 and Ca^{2+} indicator dye. In the remaining curves, simulations for the differential secretory trigger model (Scheme 1; blue lines), differential priming model (Scheme 2; green lines), and differential priming with a modified two-binding site secretory trigger (Scheme 3; red lines) are overlaid on experimental measurements from phasic synapses (filled triangles) of the following characteristics: **B**, maximum release rate; **C**, quantal content accumulated to 30 ms after the flash; **D**, time to peak release rate (**B**); **E**, delay from flash to first quantal release. **F**, Full predicted time course of the release rate for different Ca^{2+} steps for all three models overlaid on a histogram of the release rate for a phasic synapse in response to a full flash. **G**, Same as **F** but for cumulative release. The histograms have been slightly rescaled (left ordinates) to match the predicted amplitudes for the largest responses (dashed lines) to allow for better kinetic comparisons.

included a small “ Ca^{2+} spike” that is a consequence of the finite flash duration, photolysis rate, and Ca^{2+} -binding kinetics of DMNPE-4, as outlined in Materials and Methods.

In Figure 5B–E, blue lines plot the characteristics of transmitter release predicted by this scheme to the series of $[\text{Ca}^{2+}]_i$ steps. The Ca^{2+} dependence of the peak release rate (Fig. 5B), cumulative quantal release during the first 30 ms after the flash (Fig. 5C), the time to the peak release rate after the flash (Fig. 5D), and the delay from the flash to the first quantal release (Fig. 5E) are plotted along with the experimental measurements for phasic synapses. The $[\text{Ca}^{2+}]_i$ on the abscissa of each graph corresponds to the $[\text{Ca}^{2+}]_i$ measured when the flash artifact had dissipated, 50 ms after the flash, and the same time point is used in the simulated $[\text{Ca}^{2+}]_i$ steps to designate the $[\text{Ca}^{2+}]_i$ level of the step. Note that this level is less than the highest $[\text{Ca}^{2+}]_i$ reached at the end of the 7 ms flash. The peak levels calculated for flashes that produced nominal levels measured at 50 ms (in parentheses) were (in μM): 3.21 (2.89), 2.51 (2.07), 2.00 (1.52), 1.53 (1.06), 1.22 (0.805), 0.926 (0.579), 0.700 (0.428), and 0.513 (0.316).

For the same range of $[\text{Ca}^{2+}]_i$ steps, we also made more detailed comparisons of the predicted and experimentally determined time courses of release rate (Fig. 5F, blue lines) and cumulative release (Fig. 5G, blue lines) from a single terminal (gray histograms). The maximum release rate and cumulative release for this particular experiment were somewhat higher than the prediction (Fig. 5B–E, rightmost points), so the histograms are rescaled to permit better comparison of predicted and observed time courses. For all simulations, the RRP was fixed at 58 quanta, its average size in phasic synapses (Millar et al., 2002). For the parameters chosen for this simulation ($k_{\text{on}} = 1.2 \times 10^8 \text{ M/s}$; $k_{\text{off}} = 1000/\text{s}$; cooperativity factors, $a = 1$ and $b = 0.3$; Ca^{2+} stoichiometry = 5; $\gamma = 10,000/\text{s}$), the predictions show reasonable agreement with results. We explored different Ca^{2+} stoichiometries and the effects of eliminating positive cooperativity ($b = 1$) or introducing it by increasing on rates ($a > 1$) while reducing k_{on} to keep the on rate of the last step within the physical bounds imposed by Ca^{2+} dehydration before binding to coordination sites ($\sim 10^9 \text{ M/s}$). All of these alternatives produced markedly worse fits to the data.

The same reaction scheme, but with different kinetic parameters, produced a fairly good fit to release from tonic synapses (Fig. 6, blue lines). Figure 6 compares predictions to experimental data just as in Figure 5, except that Figure 6B plots cumulative release in 100 ms because responses to small $[\text{Ca}^{2+}]_i$ steps did not even begin until 30–45 ms after the flash (Fig. 6D), and even to the largest $[\text{Ca}^{2+}]_i$ steps, very little secretion occurred in the first 30 ms (Fig. 6E,F). The fit shown was obtained by reducing k_{on} to $1.7 \times 10^7 \text{ M/s}$ and k_{off} to 140/s. The slow kinetics of the responses required slower Ca^{2+} on and off rates, and this led to a more gradual exhaustion of the RRP (fixed at 130 for tonic synapses) (Millar et al., 2002) with the same basic Ca^{2+} affinity (8.3 μM) as for phasic synapses. For comparison of actual time courses of release rate and cumulative release, the number of quanta released by single flashes was too small to construct a meaningful histogram. Therefore, responses to the three largest $[\text{Ca}^{2+}]_i$ steps were lumped to form histograms of quantal release rates and cumulative release. These should be compared with a step to the average $[\text{Ca}^{2+}]_i$ reached in these three flashes, which was 2.2 μM , corresponding to the second (dashed) blue line from the top in Figure 6, E and F. The simulated release rates and cumulative release rates for different reaction schemes have been normalized to the peak value for the largest response. The simulations capture the characteristics of the experimental results reasonably well, except that release tapers off more quickly than expected, as seen from the histogram of Figure 6E and the predicted cumulative release within 100 ms (Fig. 6B).

Predicting release to action potentials

Our basic hypothesis is that differences in Ca^{2+} sensitivity to steps leading to exocytosis are responsible for the responses of phasic and tonic synapses to action potentials, whereas the local $[\text{Ca}^{2+}]_i$ -triggering release is similar. Although local $[\text{Ca}^{2+}]_i$ at the secretory trigger has not been measured, the Ca^{2+} influx per active zone is similar at phasic and tonic terminals (Moghina et al., 1999). To test this idea, we asked two questions: First, will the expected time course of $\text{Ca}(t)$ at the secretory trigger produce the observed time course of evoked transmitter release if it is used to drive Scheme 1? Second, can the magnitude of release be produced by similar levels of peak $[\text{Ca}^{2+}]_i$ at phasic and tonic synapses?

To answer these questions, we calculated responses of Scheme 1 to the expected $\text{Ca}(t)$ at secretory triggers near Ca^{2+} channels during an action potential, derived as explained in Materials and Methods; kinetic parameters were left unchanged from values used to fit phasic and tonic flash responses, respectively. Figure 7A illustrates $\text{Ca}(t)$ in the top left plot and shows responses in a phasic synapse to an action potential in the bottom left plot. The predicted release time course matched closely the time course of EJC release obtained by deconvolution of EJCs with spontaneous mEJCs at a typical synapse, and the observed quantal content (7.7) equaled that predicted from Scheme 1 using the phasic kinetic parameters, for a local $[\text{Ca}^{2+}]_i$ reaching $14.7 \mu\text{M}$. Moreover, the same $\text{Ca}(t)$ reaching a peak $15.4 \mu\text{M}$ drove Scheme 1 with the tonic kinetic parameters to generate a release time course and efficacy matching that measured from a typical tonic terminal (quantal content 0.012). The exact magnitude of local $[\text{Ca}^{2+}]_i$ rise needed to match the quantal content of release to an action potential is sensitive to small changes of release parameters, and the experimental quantal content is also variable from preparation to preparation, especially in tonic synapses. Therefore, the difference between peak $[\text{Ca}^{2+}]_i$ calculated at the secretory trigger during action potentials between tonic and phasic synapses is not significant. Scheme 1, based on different Ca^{2+} binding rates, can thus account for the differences in natural spike-evoked release, as well as the differences in response to steps of $[\text{Ca}^{2+}]_i$ between phasic and tonic synapses.

Because phasic and tonic synapses respond so differently to a train of action potentials, we decided to test whether Scheme 1 can predict the responses to such a stimulus. Figure 7A shows responses of phasic synapses in the bottom right plot to a train of five action potentials at 100 Hz, for which local $[\text{Ca}^{2+}]_i$ transients at the secretory trigger are shown in the top right plot. After a slight facilitation, depression dominates the responses as the RRP is quickly depleted. The quantal content of the fifth response is reduced to 64% that of the first action potential. When the same stimulus is used to drive Scheme 1 with the parameters used to fit

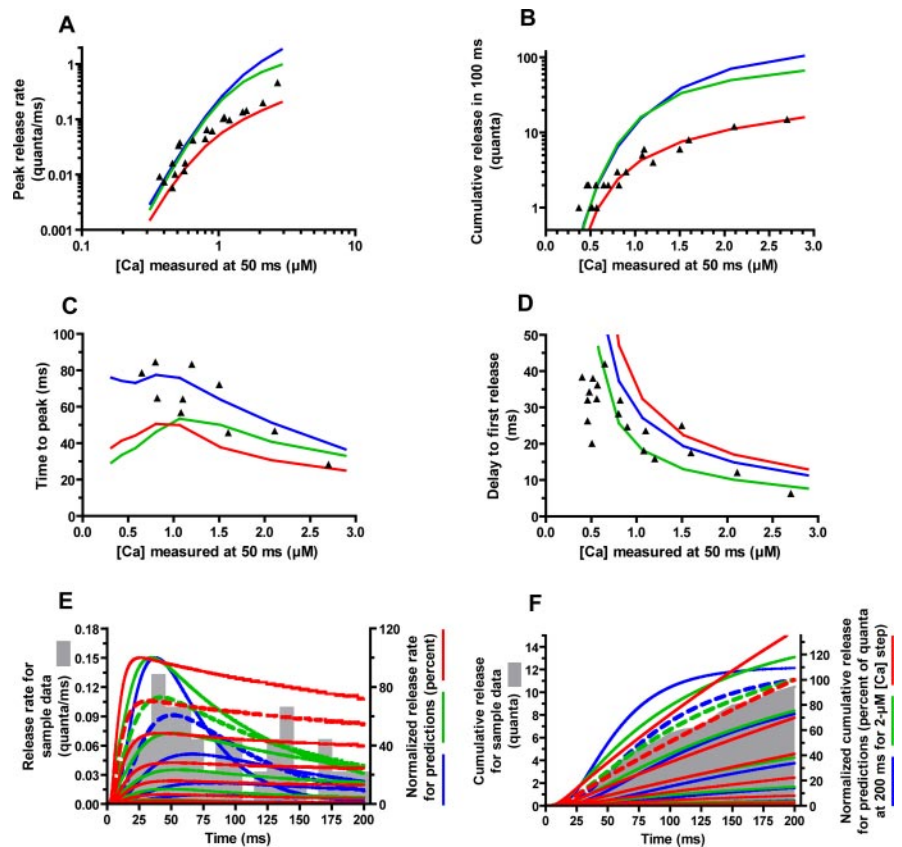


Figure 6. Characteristics of tonic synapse responses. Predictions of the three molecular schemes are compared with experimental measurements from tonic synapses (filled triangles). The same eight $\text{Ca}(t)$ waveforms used for driving phasic synapses (Fig. 5A) were used to generate these predictions for tonic synapses. In Scheme 1 (blue lines), the secretory trigger had slower Ca^{2+} -binding kinetics. In Scheme 2 (green lines), fewer vesicles in the RRP were primed in tonic synapses. In Scheme 3 (red lines), the secretory trigger was modified to allow two classes of Ca^{2+} -binding sites. **A–D**, Maximum release rate, cumulative release in the first 100 ms, time to peak release rate, and delay to first release, respectively. **E, F**, Predicted time courses of release rates and cumulative release are normalized to the maximum value for the largest response and overlaid on histograms formed from responses corresponding to the three rightmost points of **A–D**. The average $[\text{Ca}^{2+}]_i$ that evoked these responses equaled that used to generate the second highest predictions of the scheme (dashed lines), to which they should be compared. The peak levels of the predicted responses in **E** to this level of $[\text{Ca}^{2+}]_i$ were 1.12, 0.72, and 0.14 quanta/ms for the blue, green, and red dashed lines (Schemes 1–3), respectively. In **F**, predictions are normalized to the cumulative release at 200 ms for a $2 \mu\text{M}$ $[\text{Ca}^{2+}]_i$ step, which were 116, 89, and 24 quanta for Schemes 1–3, respectively.

tonic synapses, the result is quite different (Fig. 7B). A dramatic facilitation is produced, with quantal content increasing by the fifth action potential to 120 times (11,900% facilitation) that of the first. Although facilitation and depression of tonic and phasic synapses have not been characterized quantitatively, the simulated results resemble qualitatively the reported differences between the two synaptic types in response to 100 Hz stimulation (Bradacs et al., 1997; Millar et al., 2002).

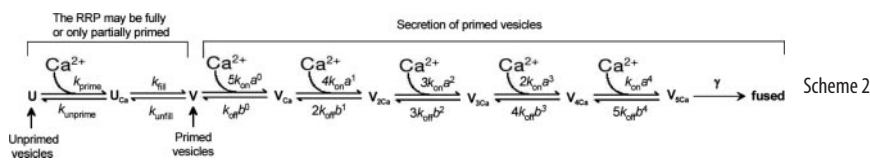
This suggested that all physiological differences between phasic and tonic synapses might arise from different Ca^{2+} -binding kinetics of the secretory trigger. However, we found a serious problem with Scheme 1 for tonic synapses: the positive cooperativity of binding successive Ca^{2+} ions and the associated reduction in the off rate slows the dissociation of Ca^{2+} ions from the secretory trigger when it is almost fully occupied ($V_{4\text{Ca}}$) to only 3.7/s, generating a huge facilitation. Simulations without positive cooperativity did not fit the data as well and required a slower k_{off} that again caused facilitation by the slow dissociation of Ca^{2+} ions after action potentials. Thus, facilitation arises in the simulations from very slow unbinding of Ca^{2+} ions from the secretory trigger, such that vesicles that were activated but not released by

the first action potential (i.e., did not quite reach state V_{5Ca}) do not return to the ground state V before the next action potential. After successive spikes, more vesicles reside at or close to state V_{4Ca} and are more readily released. Facilitation by this mechanism would be resistant to reduction by injection of exogenous Ca^{2+} buffers. This contradicts extensive evidence (Delaney et al., 1991; Hochner et al., 1991; Kamiya and Zucker, 1994) that facilitation is linked to the action of residual Ca^{2+} following action potentials acting on a separate molecular target (Zucker and Regehr, 2002). This target is either a saturable buffer (Rozov et al., 2001; Zucker and Regehr, 2002; Blatow et al., 2003; Felmy et al., 2003; Matveev et al., 2004) or one that directly regulates release (Tang et al., 2000; Matveev et al., 2002). We must therefore reject Scheme 1 because it cannot account for this aspect of the behavior of tonic synapses and seek another mechanism that differentiates tonic from phasic synapses.

Differential priming model

Much attention has been directed recently to the concept of priming synaptic vesicles for release (Neher, 1998; Martin, 2002; Rettig and Neher, 2002). It is clear that not all vesicles in nerve terminals are perched at the membrane immediately ready for release; at some terminals, only a small fraction of the total supply of vesicles can be released rapidly (to a train of spikes). This RRP may correspond to vesicles in active zones docked at the membrane (Schikorski and Stevens, 1997). Not all of these vesicles are immediately releasable because the maximum number of quanta released by an action potential can be far less than the number of docked vesicles and in some cases may be limited to only one per active zone (Stevens, 2003). The maturation of vesicles into the RRP and then to a state from which they are immediately releasable by the next action potential is often referred to as “priming.” The fraction of the RRP released by tetanic stimulation that is fully primed at rest and ready for release by a single action potential might be much higher at phasic synapses. Furthermore, the dramatic facilitation of tonic synapses might correspond to the progressive priming of vesicles during repetitive stimulation. There might be no difference in the properties of the secretory trigger per se between phasic and tonic synapses.

This idea was formulated in Scheme 2, in which a Ca-dependent priming of vesicles is included explicitly as a process distinct from and anterior to vesicle exocytosis:



Here, the RRP has been split into primed (V) and unprimed (U) vesicles, and priming is represented as having Ca^{2+} -dependent and -independent steps, corresponding to Ca -binding and subsequent conformation changes and allowing for independent regulation of kinetics, Ca^{2+} affinity, and efficacy. The hypothesis we now propose to test is that phasic and tonic synapses differ only in their state of priming, with no difference in the exocytic trigger. We implemented this model by setting the parameters for the secretory trigger to the values used in Scheme 1 for phasic synapses and seeing whether, by altering the parameters regulating priming, we could replicate the behaviors of the two types of synapses.

Figure 5 shows the predictions of this scheme for phasic syn-

apses as green lines, with $k_{prime} = 4 \times 10^8$ M/s, $k_{unprime} = 50/s$, $k_{fill} = 500/s$, and $k_{unfill} = 50/s$. At rest ($[Ca^{2+}]_i = 100$ nM), 82% of the RRP is primed, and the simulations are almost indistinguishable from the blue lines of Scheme 1. For tonic synapses, the priming parameters were adjusted so that $k_{prime} = 8 \times 10^6$ M/s, $k_{unprime} = 50/s$, $k_{fill} = 50/s$, and $k_{unfill} = 50/s$, which leaves only 1.5% of the RRP primed at rest. The Ca^{2+} affinity of the priming site was reduced from 125 nM to 6.25 μ M, and the second step, which might represent the filling of release sites by primed vesicles, was altered to reduce the proportion of vesicles activated by Ca^{2+} that are fully primed (“efficacy of priming”). The results are shown as green lines in Figure 6. The simulations provide a satisfactory fit to the data, slightly better than Scheme 1 in some respects (e.g., delay to first release) and slightly worse in others (e.g., time to peak), suggesting that a different state of priming might in fact be a major difference between phasic and tonic synapses.

Next, we wanted to see whether Scheme 2 could also explain the responses of phasic and tonic synapses to action potentials. To do this, we must consider where in the nerve terminal priming occurs and, in particular, where the Ca^{2+} -sensitive step is located with respect to the Ca^{2+} channels. It has been pointed out previously (Tang et al., 2000; Matveev et al., 2002) that if a Ca^{2+} process with high affinity were exposed to the local high $[Ca^{2+}]_i$ in the microdomains triggering secretion (Neher, 1998), the site would be saturated after each action potential, and there would be no progressive effect on synaptic transmission. Therefore, we assume that Ca^{2+} primes vesicles at a site more distant from the nearest Ca^{2+} channel, perhaps 100–150 nm away in diffusional distance, which might be physically considerably closer because of restricted diffusion and tortuosity in the crowded space at the base of docked vesicles. We have borrowed the results of previous calculations of $Ca(t)$ at such a location at crayfish motor nerve terminals during a 100 Hz train. We used a $Ca(t)$ profile that is half that shown for 100 nm from the nearest Ca^{2+} channel of Matveev et al. (2002), their Figure 1, which is what we might expect for $[Ca^{2+}]_i \sim 150$ nm away. This slowly rising and decaying “residual Ca^{2+} ,” which accumulates during a train, is shown as orange traces in Figure 7, *C* and *D*. A similar waveform, arising from channels more distant than those producing the microdomain surrounding docked vesicles, is added to the Gaussian (see Materials and Methods) representing the local microdomain Ca^{2+} to produce the total $Ca(t)$ at the secretory trigger.

Considering first a single action potential, we were able to replicate the time course and magnitude of spike-evoked release at both phasic and tonic synapses with this scheme; a peak $[Ca^{2+}]_i$ reaching 15.0 μ M at the secretory trigger released 7.7 quanta in phasic simulations, matching the quantal content of the phasic terminal recorded in Figure 7*C*. The initial quantal content at a tonic terminal (0.012) and its time course of release were matched by using the parameters derived from fitting Scheme 2 to Ca^{2+} steps at tonic synapses, but now a peak $[Ca^{2+}]_i$ of only 5.5 μ M was required. Thus, if this scheme is accepted, it might imply that tonic action potentials at tonic synapses generate a smaller peak $[Ca^{2+}]_i$ at the secretory trigger than at phasic synapses. The differences in short-term plasticity were also preserved: phasic terminals depressed to one-fifth the initial quantal content by the fifth spike, whereas tonic terminals facilitated 98-fold (9700%).

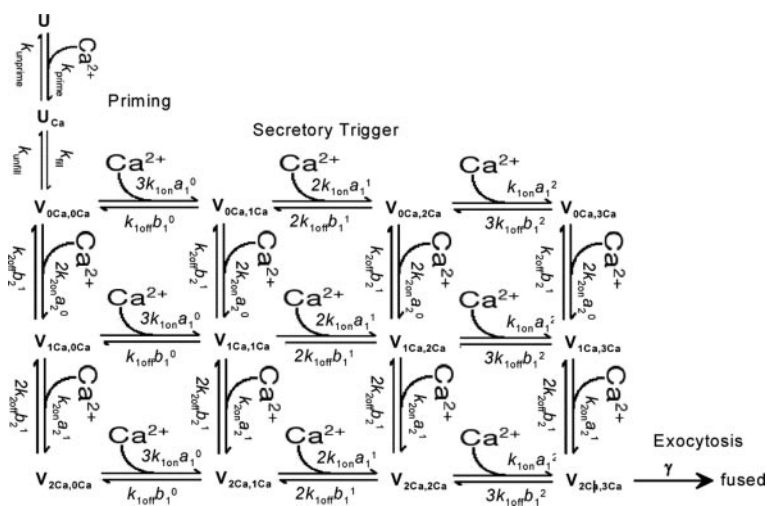
The chief difficulty with these simulations lies in the interspike

intervals. At simulated phasic synapses, transmitter release persists at a rate of ~2–3 quanta/ms between action potentials; this is much higher than what is observed experimentally (Millar et al., 2002). At tonic synapses, release continues at the same rate or even higher than the evoked release right after the first action potential (at 0.2 quanta/ms) (Fig. 7D, bottom right plot). Thus, transmission is not timed to occur mainly right after the action potential, again contradicting experimental observation, and Scheme 2 also suffers from a major flaw.

This behavior is attributable to the positive cooperativity of successive Ca²⁺ bindings at the secretory trigger. Once the high energy barrier of the first couple of Ca²⁺ bindings is overcome, the small (micromolar) residual Ca²⁺ persisting at release sites is sufficient to bind to the remaining high-affinity step(s) and drive to secretion those vesicles that were nearly released by the Ca²⁺ microdomain of the previous action potential. Moreover, the increasingly slow off rate prevents the Ca²⁺ ions that have bound from falling off before others from the residual Ca²⁺ can bind. This problem applies equally to Scheme 1 (data not shown) because it is a characteristic of the secretory trigger with positive cooperativity and multiple sequential Ca²⁺ binding steps. We conclude that Scheme 2 must also be rejected.

Modification of the secretory trigger

The problem with Scheme 2 arose from the sequential binding of five Ca²⁺ ions with positive cooperativity (progressively slowing off rate). However, this does not seem to be a realistic model for Ca²⁺ binding to synaptotagmin, the putative secretory trigger. Synaptotagmin binds three Ca²⁺ ions at its C2A domain and two at its C2B domain (Bai and Chapman, 2004), and both domains participate in Ca²⁺-regulated secretion (Stevens and Sullivan, 2003). Although, in principle, Ca²⁺ ions could bind sequentially to one domain before the other, it is more likely that binding to C2A and C2B domains proceeds independently, starting with similar affinities at each site. These considerations prompted a modification to the above schemes; we allowed Ca²⁺ ions to bind simultaneously at the two sites but sequentially at each site with positive cooperativity:



In Scheme 3, there are two classes of Ca²⁺-binding sites, with separate initial on and off rates (k_{1on} and k_{1off} , k_{2on} and k_{2off}) and forward and backward cooperativity factors (a_1 and b_1 , a_2 and b_2).

We implemented this scheme for phasic synapses by choosing the following parameters: $k_{prime} = 1.0 \times 10^8$ M/s, $k_{unprime} = 50$ /s;

$k_{fill} = 5000$ /s, $k_{unfill} = 500$ /s, $k_{1on} = k_{2on} = 1.2 \times 10^8$ M/s, $k_{1off} = k_{2off} = 125$ /s, $a_1 = a_2 = 1$, $b_1 = b_2 = 0.5$, and $\gamma = 10,000$ /s. For simplicity, we explored only parameter sets with identical binding constants for the first Ca²⁺ ion to each of the two classes of binding sites and identical positive cooperativity factors. The results of the simulation are shown as red lines in Figure 5B–G. This scheme describes the data as well as the previous two.

For tonic synapses, we obtained a reasonable fit to the data using the identical secretory trigger parameters, but with the following priming site values: $k_{prime} = 6.0 \times 10^5$ M/s, $k_{unprime} = 40$ /s, $k_{fill} = 800$ /s, and $k_{unfill} = 800$ /s, producing the red lines in Figure 6. The predicted peak release rates and cumulative releases fit the data better than Schemes 1 and 2, whereas the times to peak and delays to first release are not quite as good. These parameters leave only 0.15% of the RRP in a fully primed state, compared with 62.5% for the parameters used for phasic synapses. From Figure 6, E and F, the time courses of release and cumulative release are best described by Scheme 3, which is not evident from the fits of individual characteristics of Figure 6B–E. The histogram in Figure 6E emphasizes the lack of precision when working with tonic synapses in estimating characteristics such as peak release rate and time to peak used for the plots of Figure 6, B and D.

The behavior of Scheme 3 for single action potentials and for five spikes at 100 Hz is shown in Figure 7, E and F. Initial quantal content and release time course at the phasic synapse were matched with a peak $[Ca^{2+}]_i$ of 16.9 μ M at the secretory trigger; at tonic synapses, a good match was achieved with a peak $[Ca^{2+}]_i$ of 10.9 μ M. Simulations of the phasic synapses exhibited a strong depression, to 21% of the initial quantal content, whereas the tonic synapse simulations facilitated to 28 times the initial release level (2700% facilitation). These simulations resemble the depression and facilitation that were observed experimentally (Millar et al., 2002).

In these simulations, facilitation arises from the priming action of residual Ca²⁺, rather than from a slow kinetic rate constant as in Scheme 1. This may be seen by omitting the priming steps from this scheme, in which case facilitation reached only 268% (data not shown). Depression arises from depletion of the

RRP, recovery from which is not included in these simulations. The problem of a large persistent transmitter release in the interspike interval of Scheme 2 as applied to tonic synapses is alleviated. The predicted increase in spontaneous quantal release frequency, to ~1 quantum per 20 trials in the 10 ms interval between spikes, resembles what we have observed qualitatively during repetitive stimulation (A. G. Millar, unpublished observations). In conclusion, Scheme 3 provides the best replication yet for the full constellation of differences in release properties of phasic and tonic synapses.

Discussion

Our key finding is a large difference in the Ca²⁺ sensitivity and kinetics of the transmitter release machinery between phasic and tonic synapses in response to step rises in $[Ca^{2+}]_i$. As pointed out in Introduction, no other property has been found differentiating the two synaptic types that could explain the much stronger efficacy of release from phasic boutons to a single action potential. In the second part of our study, we found that three

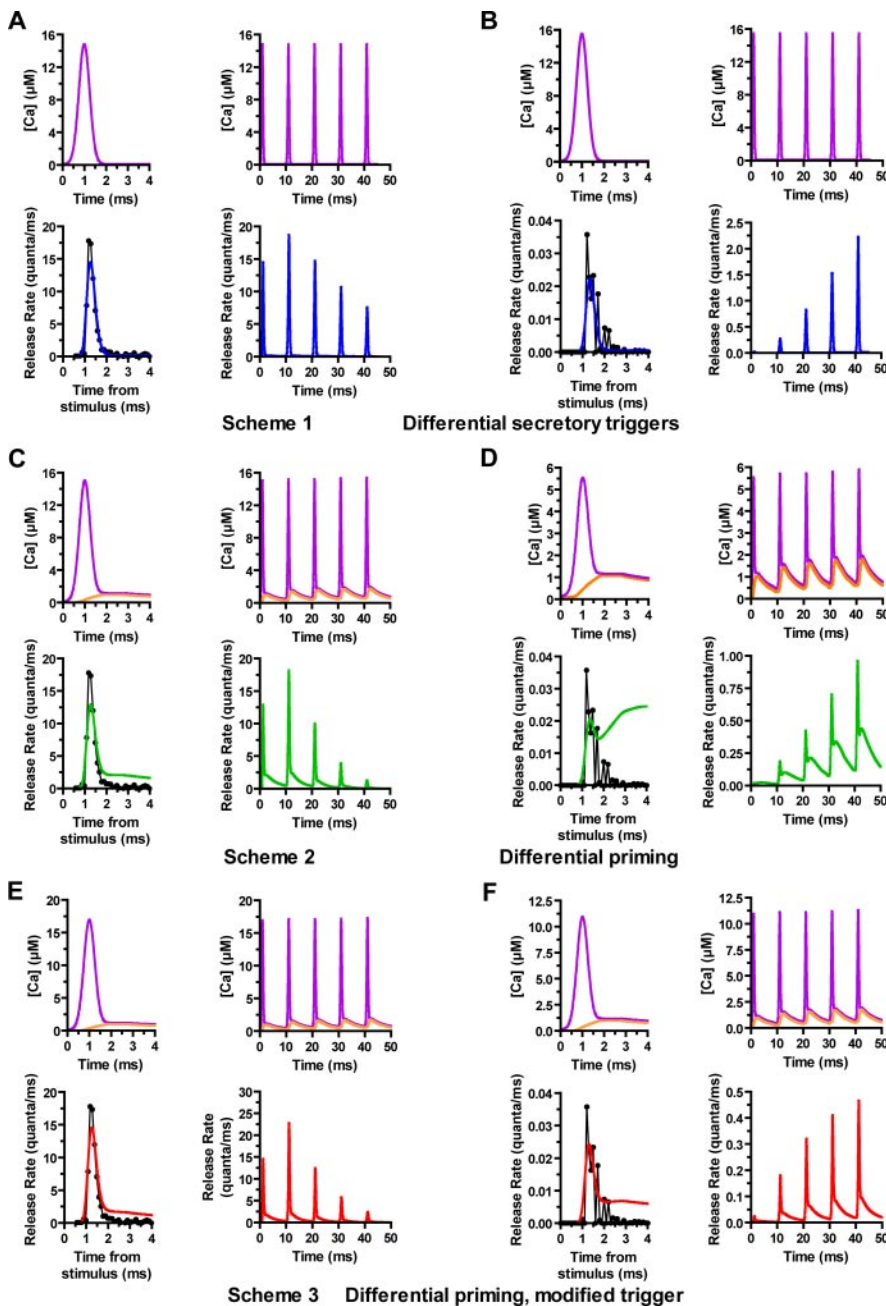


Figure 7. Simulated responses of three molecular schemes to one spike and to a 100 Hz train of action potentials and comparison with measured time course of release evoked by one action potential. Phasic synapses are shown on the left (**A, C, E**); tonic synapses are shown on the right (**B, D, F**). **A, B**, Simulations for Scheme 1 in blue. **B, C**, Simulations for Scheme 2 in green. **E, F**, Simulations for Scheme 3 in red. In each plot, the top row shows the time course of $Ca(t)$ at the secretory trigger in purple, to a single action potential at an expanded time scale on the left, and to a train of five spikes at a compressed time scale on the right. Transmitter release to these stimuli is shown directly below them. In simulations that include priming (**C–F**), $Ca(t)$ at the putative priming site is also shown in orange, and this residual Ca^{2+} is included in $Ca(t)$ at the secretory trigger.

molecular reaction schemes could describe the kinetics and magnitudes of release to a series of $[Ca^{2+}]_i$ steps and could account for the responses to single spikes and trains of action potentials at phasic and tonic synapses.

We began by with a scheme of the sequential binding of up to five Ca^{2+} ions to a secretory trigger, followed by a fusion step. This scheme accounted reasonably well for the properties of responses to step rises in $[Ca^{2+}]_i$, to the expected time course of local $[Ca^{2+}]_i$ during an action potential, and to trains of five action potentials. The phasic synapses resemble many vertebrate

synapses at which depression dominates, and our parameter values are similar to those for this scheme at the calyx of Held (Bollmann et al., 2000; Schneggenburger and Neher, 2000). Applying the first scheme to tonic synapses assumed differences in Ca^{2+} -binding properties of the secretory trigger. Initially, we imagined that tonic synapses bind Ca^{2+} with lower affinity than phasic synapses, making them less sensitive to $[Ca^{2+}]_i$. Such a reduced affinity could arise, for example, from faster Ca^{2+} dissociation rates from the secretory trigger. In that case, facilitation would not have arisen from Scheme 1, and we would have attributed it to some independent process. However, we were unable to fit the results of our experiments on $[Ca^{2+}]_i$ steps by reducing Ca^{2+} -binding affinity, whether by increasing Ca^{2+} dissociation rates or increasing Ca^{2+} association rates; instead, we could only fit the results by reducing both on and off rates for Ca^{2+} binding, i.e., by slowing the kinetics of Ca^{2+} binding. Under these conditions, facilitation to a train of action potentials arose from the slow dissociation of Ca^{2+} , contradicting evidence that facilitation is attributable to residual Ca^{2+} .

The second scheme attributed the difference between synapse types to different Ca^{2+} sensitivities and resting states of priming, with most vesicles in the RRP unprimed at rest in tonic synapses. This scheme could also account for most aspects of responses to steps in $[Ca^{2+}]_i$, but it predicted too high an increase in asynchronous release at tonic synapses. In this situation, trigger molecules with three or four Ca^{2+} ions bound were too sensitive to residual Ca^{2+} because of the increasing Ca^{2+} affinities of successive binding steps.

The third scheme was a variant of the priming model in which a modified secretory trigger with Ca^{2+} binding independently at two binding sites was used, more in keeping with the Ca^{2+} -binding structure of synaptotagmin. This scheme provided the best description of the different responses to Ca^{2+} steps and action potentials, as well as short-term plasticity and asynchronous release, at phasic and tonic synapses. The Ca^{2+} association rate derived by fitting this scheme to our data (1.2×10^8 M/s) is similar to estimates from kinetic studies of Ca^{2+} binding to the C2A domain of synaptotagmin (4×10^7 – 1×10^8 M/s) (Davis et al., 1999; Millet et al., 2002); moreover, binding of Ca^{2+} to C2A and C2B domains appears to be similar, which was a simplifying assumption in our choice of parameters. In this scheme, facilitation arises from the priming of vesicles by Ca^{2+} (Worden et al., 1997) acting at a site relatively distant from a Ca^{2+} channel and as such is a variant of the two-site model of facilitation (Tang et al., 2000; Matveev et al., 2002). This new scheme may be closer to what is actually happening at synaptic terminals.

A finding of general importance is that Scheme 1 also produces too high an asynchronous release rate when the effects of residual Ca^{2+} are considered. Thus, incorporating residual Ca^{2+} at the release trigger into simulations of Scheme 1 generates a large interspike release similar to those shown in the bottom left plots of Figure 7, *C* and *D* (simulation not shown). This might be a problem for any preparation in which Scheme 1 has been applied (Heidelberger et al., 1994; Bollmann et al., 2000; Schneggenburger and Neher, 2000; Beutner et al., 2001; Felmy et al., 2003) but has not been noted because previous applications of Scheme 1 did not specifically treat the effects of residual Ca^{2+} on asynchronous release between action potentials. Scheme 3, which attempted to incorporate Ca^{2+} -binding features of synaptotagmin in the way that Ca^{2+} bound to the secretory trigger, may therefore also be valuable in modeling release at other synapses.

Preliminary experimental results support the concept of Ca^{2+} -dependent priming at tonic synapses. When maximal release rates are imposed by pretreatment with Cs^+ and high-frequency stimulation (Millar et al., 2002), quantal release always facilitates for a few impulses before attaining a maximal value and then depressing. This effect may be attributable to a priming process initiated early in the train of stimuli. In contrast, phasic synapses do not show an initial priming phase during production of maximal release in Cs^+ -treated terminals. Steady presynaptic depolarization of tonic nerve endings also potentiates release by action potentials, presumably by increasing steady-state intracellular Ca^{2+} (Wojtowicz and Atwood, 1983, 1984). When tonic nerve endings are injured by pressure from a macropatch electrode, resting $[\text{Ca}^{2+}]_i$ rises, and action potential-evoked release increases. These observations, although incomplete, suggest a Ca^{2+} -dependent priming process, which can increase evoked release at tonic synapses, in support of the priming-dependent reaction schemes presented here.

Alternative formulations of priming to those presented here might also be used to model the data. Phasic synapses were modeled as “preprimed” because of a higher Ca^{2+} -affinity of the priming step; we could equally well have assumed that, at phasic synapses, the priming process is simply absent. Alternatively, we could imagine that only tonic synapses contain a special brake on priming that is relieved by Ca^{2+} . It is also possible that priming acts in parallel or simultaneously with the secretory process (Yamada and Zucker, 1992) rather than anterior to it. Furthermore, our modification of the secretory trigger in Scheme 3 is only the simplest of several we could think of. For example, the two binding sites envisaged in the secretory trigger may have different Ca^{2+} -binding kinetics, multiple synaptotagmins may participate in vesicle release (Hua and Scheller, 2001), and vesicles may be heterogeneous in their release probabilities (Trommershäuser et al., 2003). Thus, the exact details of Scheme 3 remain to be substantiated and may be modified in light of additional data. The major point of the modeling is the demonstration that only a difference in the Ca^{2+} dependence of priming can explain all the differences between tonic and phasic synapses.

The present results beg the question of the identity of the priming molecule(s). Popular candidates include munc13, rab3-interacting molecule, rabphilin, synapsin/Ca-calmodulin-dependent kinase, SNAP-25 (synaptosome-associated protein of 25 kDa), and neuronal calcium sensor-1 (Geppert and Südhof, 1998; Hilfiker et al., 1999; Duncan et al., 2000; Lonart, 2002; Martin, 2002; Rettig and Neher, 2002; Zucker, 2003; Heidelberger and Matthews, 2004). Because we are suggesting that the same molecule(s) may be responsible for synaptic facilitation, their identification and characterization become doubly important. A further mystery is how the molecular machinery control-

ling the differences between phasic and tonic synapses is regulated. A clue is provided by the discovery that different terminals of a single neuron can display widely different degrees of facilitation and initial release probability that appear to be target-dependent (Atwood, 1967; Bittner, 1968; Atwood and Bittner, 1971; Markram et al., 1998; Reyes et al., 1998), suggesting posttranscriptional and perhaps posttranslational presynaptic modifications under postsynaptic regulation. In the case of crayfish junctions from different motor neurons with very different properties projecting onto the same target, postsynaptic regulation would not seem to be the defining mechanism.

References

- Araque A, Clarac F, Buno W (1994) P-type Ca^{2+} channels mediate excitatory and inhibitory synaptic transmitter release in crayfish muscle. *Proc Natl Acad Sci USA* 91:4224–4228.
- Atwood HL (1967) Variation in physiological properties of crustacean motor synapses. *Nature* 215:57–58.
- Atwood HL, Bittner GD (1971) Matching of excitatory and inhibitory inputs to crustacean muscle fibers. *J Neurophysiol* 34:157–170.
- Atwood HL, Karunanithi S (2002) Diversification of synaptic strength: presynaptic elements. *Nat Rev Neurosci* 3:497–516.
- Augustine GJ, Santamaria F, Tanaka K (2003) Local calcium signaling in neurons. *Neuron* 40:331–346.
- Bai J, Chapman ER (2004) The C2 domains of synaptotagmin: partners in exocytosis. *Trends Biochem Sci* 29:143–151.
- Beutner D, Voets T, Neher E, Moser T (2001) Calcium dependence of exocytosis and endocytosis at the cochlear inner hair cell afferent synapse. *Neuron* 29:681–690.
- Bittner GD (1968) Differentiation of nerve terminals in the crayfish opener muscle and its functional significance. *J Gen Physiol* 51:731–758.
- Blatow M, Caputi A, Burnashev N, Monyer H, Rozov A (2003) Ca^{2+} buffer saturation underlies paired pulse facilitation in calbindin-D28k-containing terminals. *Neuron* 38:79–88.
- Blundon JA, Wright SN, Brodwick MS, Bittner GD (1995) Presynaptic calcium-activated potassium channels and calcium channels at a crayfish neuromuscular junction. *J Neurophysiol* 73:178–189.
- Bollmann JH, Sakmann B, Borst JG (2000) Calcium sensitivity of glutamate release in a calyx-type terminal. *Science* 289:953–957.
- Bradacs H, Cooper RL, Msghina M, Atwood HL (1997) Differential physiology and morphology of phasic and tonic motor axons in a crayfish limb extensor muscle. *J Exp Biol* 200:677–691.
- Cooper RL, Stewart BA, Wojtowicz JM, Wang S, Atwood HL (1995) Quantal measurement and analysis methods compared for crayfish and *Drosophila* neuromuscular junctions and rat hippocampus. *J Neurosci Methods* 61:67–78.
- Davis AF, Bai J, Fasshauer D, Wolowick MJ, Lewis JL, Chapman ER (1999) Kinetics of synaptotagmin responses to Ca^{2+} and assembly with the core SNARE complex onto membranes. *Neuron* 24:363–376.
- Delaney K, Tank DW, Zucker RS (1991) Presynaptic calcium and serotonin-mediated enhancement of transmitter release at crayfish neuromuscular junction. *J Neurosci* 11:2631–2643.
- Dobrunz LE, Stevens CF (1997) Heterogeneity of release probability, facilitation, and depletion at central synapses. *Neuron* 18:995–1008.
- Dudel J (1981) The effect of reduced calcium on quantal unit current and release at the crayfish neuromuscular junction. *Pflügers Arch* 391:35–40.
- Duncan RR, Shipston MJ, Chow RH (2000) Double C2 protein: a review. *Biochimie* 82:421–426.
- Ellis-Davies GC (2003) Development and application of caged calcium. *Methods Enzymol* 360:226–238.
- Ellis-Davies GC, Kaplan JH, Barsotti RJ (1996) Laser photolysis of caged calcium: rates of calcium release by nitrophenyl-EGTA and DM-nitrophen. *Biophys J* 70:1006–1016.
- Felmy F, Neher E, Schneggenburger R (2003) Probing the intracellular calcium sensitivity of transmitter release during synaptic facilitation. *Neuron* 37:801–811.
- Geppert M, Südhof TC (1998) RAB3 and synaptotagmin: the yin and yang of synaptic membrane fusion. *Annu Rev Neurosci* 21:75–95.
- Grimes JH, Huggard AJ, Wilford SP (1963) The stabilities of the alkaline earth chelate of some polyaminopolycarboxylic acids. *J Inorg Nucl Chem* 25:1225–1238.

- Gryniewicz G, Poenie M, Tsien RY (1985) A new generation of Ca^{2+} indicators with greatly improved fluorescence properties. *J Biol Chem* 260:3440–3450.
- Heidelberger R, Matthews G (2004) Vesicle priming and depriming: a SNAP decision. *Neuron* 41:311–313.
- Heidelberger R, Heinemann C, Neher E, Matthews G (1994) Calcium dependence of the rate of exocytosis in a synaptic terminal. *Nature* 371:513–515.
- Hilfiker S, Pieribone VA, Czernik AJ, Kao HT, Augustine GJ, Greengard P (1999) Synapsins as regulators of neurotransmitter release. *Philos Trans R Soc Lond B Biol Sci* 354:269–279.
- Hochner B, Parnas H, Parnas I (1991) Effects of intra-axonal injection of Ca^{2+} buffers on evoked release and on facilitation in the crayfish neuromuscular junction. *Neurosci Lett* 125:215–218.
- Hua Y, Scheller RH (2001) Three SNARE complexes cooperate to mediate membrane fusion. *Proc Natl Acad Sci USA* 98:8065–8070.
- Kamiya H, Zucker RS (1994) Residual Ca^{2+} and short-term synaptic plasticity. *Nature* 371:603–606.
- Kao JP, Tsien RY (1988) Ca^{2+} binding kinetics of fura-2 and azo-1 from temperature-jump relaxation measurements. *Biophys J* 53:635–639.
- Kennedy D, Takeda K (1965a) Reflex control of abdominal flexor muscles in the crayfish. I. The twitch system. *J Exp Biol* 43:211–227.
- Kennedy D, Takeda K (1965b) Reflex control of abdominal flexor muscles in the crayfish. II. The tonic system. *J Exp Biol* 43:229–246.
- King MJ, Atwood HL, Govind CK (1996) Structural features of crayfish phasic and tonic neuromuscular terminals. *J Comp Neurol* 372:618–626.
- Llinás R, Steinberg IZ, Walton K (1981) Presynaptic calcium currents in squid giant synapse. *Biophys J* 33:289–321.
- Llinás R, Sugimori M, Simon SM (1982) Transmission by presynaptic spike-like depolarization in the squid giant synapse. *Proc Natl Acad Sci USA* 79:2415–2419.
- Lonart G (2002) RIM1: an edge for presynaptic plasticity. *Trends Neurosci* 25:329–332.
- Markram H, Wang Y, Tsodyks M (1998) Differential signaling via the same axon of neocortical pyramidal neurons. *Proc Natl Acad Sci USA* 95:5323–5328.
- Martin TF (2002) Prime movers of synaptic vesicle exocytosis. *Neuron* 34:9–12.
- Matveev V, Sherman A, Zucker RS (2002) New and corrected simulations of synaptic facilitation. *Biophys J* 83:1368–1373.
- Matveev V, Zucker RS, Sherman A (2004) Facilitation through buffer saturation: constraints on endogenous buffering properties. *Biophys J* 86:2691–2709.
- Millar AG, Bradacs H, Charlton MP, Atwood HL (2002) Inverse relationship between release probability and readily releasable vesicles in depressing and facilitating synapses. *J Neurosci* 22:9661–9667.
- Millet O, Bernadó P, García J, Rizo J, Pons M (2002) NMR measurement of the off rate from the first calcium-binding site of the synaptotagmin I C_2A domain. *FEBS Lett* 516:93–96.
- Msghina M, Govind CK, Atwood HL (1998) Synaptic structure and transmitter release in crustacean phasic and tonic motor neurons. *J Neurosci* 18:1374–1382.
- Msghina M, Millar AG, Charlton MP, Govind CK, Atwood HL (1999) Calcium entry related to active zones and differences in transmitter release at phasic and tonic synapses. *J Neurosci* 19:8419–8434.
- Neher E (1998) Vesicle pools and Ca^{2+} microdomains: new tools for understanding their roles in neurotransmitter release. *Neuron* 20:389–399.
- Neher E, Zucker RS (1993) Multiple calcium-dependent processes related to secretion in bovine chromaffin cells. *Neuron* 10:21–30.
- Oheim M, Naraghi M, Muller TH, Neher E (1998) Two dye two wavelength excitation calcium imaging: results from bovine adrenal chromaffin cells. *Cell Calcium* 24:71–84.
- Ohnuma K, Whim MD, Fetter RD, Kaczmarek LK, Zucker RS (2001) Presynaptic target of Ca^{2+} action on neuropeptide and acetylcholine release in *Aplysia californica*. *J Physiol (Lond)* 535:647–662.
- Ravin R, Spira ME, Parnas H, Parnas I (1997) Simultaneous measurement of intracellular Ca^{2+} and asynchronous transmitter release from the same crayfish bouton. *J Physiol (Lond)* 501:251–262.
- Rettig J, Neher E (2002) Emerging roles of presynaptic proteins in Ca^{++} -triggered exocytosis. *Science* 298:781–785.
- Reyes A, Lujan R, Rozov A, Burnashev N, Somogyi P, Sakmann B (1998) Target-cell-specific facilitation and depression in neocortical circuits. *Nat Neurosci* 1:279–285.
- Roberts WM (1994) Localization of calcium signals by a mobile calcium buffer in frog saccular hair cells. *J Neurosci* 14:3246–3262.
- Rozov A, Burnashev N, Sakmann B, Neher E (2001) Transmitter release modulation by intracellular Ca^{2+} buffers in facilitating and depressing nerve terminals of pyramidal cells in layer 2/3 of the rat neocortex indicates a target cell-specific difference in presynaptic calcium dynamics. *J Physiol (Lond)* 531:807–826.
- Schikorski T, Stevens CF (1997) Quantitative ultrastructural analysis of hippocampal excitatory synapses. *J Neurosci* 17:5858–5867.
- Schneggenburger R, Neher E (2000) Intracellular calcium dependence of transmitter release rates at a fast central synapse. *Nature* 406:889–893.
- Stevens CF (2003) Neurotransmitter release at central synapses. *Neuron* 40:381–388.
- Stevens CF, Sullivan JM (2003) The synaptotagmin C2A domain is part of the calcium sensor controlling fast synaptic transmission. *Neuron* 39:299–308.
- Tang Y, Schlumpberger T, Kim T, Lueker M, Zucker RS (2000) Effects of mobile buffers on facilitation: experimental and computational studies. *Biophys J* 78:2735–2751.
- Tank DW, Regehr WG, Delaney KR (1995) A quantitative analysis of presynaptic calcium dynamics that contribute to short-term enhancement. *J Neurosci* 15:7940–7952.
- Trommershäuser J, Schneggenburger R, Zippelius A, Neher E (2003) Heterogeneous presynaptic release probabilities: functional relevance for short-term plasticity. *Biophys J* 84:1563–1579.
- Van der Kloot W (1988) Estimating the timing of quantal releases during end-plate currents at the frog neuromuscular junction. *J Physiol (Lond)* 402:595–603.
- Wojtowicz JM, Atwood HL (1983) Maintained depolarization of synaptic terminals facilitates nerve-evoked transmitter release at a crayfish neuromuscular junction. *J Neurobiol* 14:385–390.
- Wojtowicz JM, Atwood HL (1984) Presynaptic membrane potential and transmitter release at the crayfish neuromuscular junction. *J Neurophysiol* 52:99–113.
- Wojtowicz JM, Marin L, Atwood HL (1994) Activity-induced changes in synaptic release sites at the crayfish neuromuscular junction. *J Neurosci* 14:3688–3703.
- Worden MK, Bykhovskaia M, Hackett JT (1997) Facilitation at the lobster neuromuscular junction: a stimulus-dependent mobilization model. *J Neurophysiol* 78:417–428.
- Wright SN, Brodwick MS, Bittner GD (1996) Presynaptic calcium currents at voltage-clamped excitator and inhibitor nerve terminals of crayfish. *J Physiol (Lond)* 496:347–361.
- Xu T, Naraghi M, Kang H, Neher E (1997) Kinetic studies of Ca^{2+} binding and Ca^{2+} clearance in the cytosol of adrenal chromaffin cells. *Biophys J* 73:532–545.
- Yamada WM, Zucker RS (1992) Time course of transmitter release calculated from simulations of a calcium diffusion model. *Biophys J* 61:671–682.
- Zhong N, Beaumont V, Zucker RS (2001) Roles for mitochondrial and reverse mode $\text{Na}^+/\text{Ca}^{2+}$ exchange and the plasmalemma Ca^{2+} ATPase in post-tetanic potentiation at crayfish neuromuscular junctions. *J Neurosci* 21:9598–9607.
- Zucker R (1994) Photorelease techniques for raising or lowering intracellular Ca^{2+} . *Methods Cell Biol* 40:31–63.
- Zucker RS (1992) Effects of photolabile calcium chelators on fluorescent calcium indicators. *Cell Calcium* 13:29–40.
- Zucker RS (2003) NCS-1 stirs somnolent synapses. *Nat Neurosci* 6:1006–1008.
- Zucker RS, Regehr WG (2002) Short-term synaptic plasticity. *Annu Rev Physiol* 64:355–405.
- Zucker RS, Kullmann DM, Bennett M (1999) Release of neurotransmitters. In: *Fundamental neuroscience* (Zigmond MJ, Bloom FL, Landis SC, Roberts JL, Squire LR, eds), pp 155–192. San Diego: Academic.